Journal of Catalysis 270 (2010) 256–267

Contents lists available at ScienceDirect

Journal of Catalysis

journal homepage: www.elsevier.com/locate/jcat

In situ DRIFT–TRM study of simultaneous NO_x and soot removal over Pt–Ba and Pt–K NSR catalysts

I.S. Pieta, M. García-Diéguez, C. Herrera, M.A. Larrubia, L.J. Alemany *

Department of Chemical Engineering, Faculty of Science, Campus of Teatinos, University of Malaga, E-29071 Malaga, Spain

ARTICLE INFO

Article history:
Received 3 November 2009
Revised 30 December 2009
Accepted 2 January 2010
Available online 2 February 2010

Keywords:
Soot removal
NO_x storage
LTN trap
DRIFT–TRM
Pt–Ba/Al_2O_3
Pt–K/Al_2O_3

ABSTRACT

The Pt–Ba/γ-Al_2O_3 and Pt–K/γ-Al_2O_3 catalysts have been studied in simultaneous NO_x and soot removal under cyclic lean-rich conditions. The DRIFT–TRM activity studies were accompanied by a detailed TEM/HRTEM, XRD, and XPS characterization of the catalysts samples. It was found that the alkali component stabilizes the Pt^0/Pt_{ox} ratio and better catalyst performance during simultaneous removal of NO_x and soot was obtained for Pt–Ba, where Pt^0/Pt_{ox} ratio was close to 0.70. Moreover, the NO to NO_2 oxidation rate was higher for the Pt–Ba catalyst than that for the Pt–K catalyst. The study reveals that soot has an influence both on the catalyst accumulation capacity and on the catalyst regeneration. As it is shown in the present work, the amount of NO_x stored during the lean phase of TRM increases gradually during soot removal from the catalytic system. The regeneration process depends on alkali element type and is limited for the Pt–K catalyst.

1. Introduction

The fuel efficiency, reliability and durability have made Diesel engines even more popular in the commercial market in recent years [1–9]. The enhanced oxidation improves the thermal efficiency of these engines, reduces fuel consumption, and decreases significantly the CO emission in comparison with gasoline engines. However, the same factors are responsible for the increase in NO_x and particulate matter (PM) emission, which is related to serious environmental and health problems [1,2,10–13]. Therefore, the decrease in the NO_x and PM emission from Diesel exhaust gases is one of the most important environmental issues [14–20]. Many systems have been proposed for NO_x and soot removal, but the aspect of the simultaneous emission control, especially at low temperature, is still an open debate [21–23]. NO_x storage–reduction catalysts (NSR) offer one method of controlling Diesel passenger car NO_x emission by operating under cyclic lean-rich conditions. This technique, called DPNR (Diesel Particulate NO_x Removal) technology, was proposed by Toyota in the 1990s [24]. This process is based on the NSR (or LNT lean NO_x trap) catalytic material usage, which normally operates in cyclic lean-rich conditions [6–8,12,16,17,20,25–28]. During lean period of work, NO_x is trapped over the catalyst as different type nitrates and nitrites, which are progressively transformed into nitrates upon oxidation condition [5,29,30]. This step is also accompanied by soot oxidation. The catalyst surface properties are regenerated by reduction of the stored NO_x to N_2 during short rich period.

Many catalyst formulations have been investigated with various conditions and using various reactant agents [6,7,17,25,31]. One of the most studied and promising composition of the NSR catalyst is a Pt–Ba system supported on γ-Al_2O_3 [23,25,26,32]. A lot of studies have been done considering the catalyst standard formulation Pt:AE:Al_2O_3 ≈ 1:20:100 (AE – alkali element); however, there is still a need to improve the catalysts composition and to optimize the catalytic process [6,7,16,31–33]. There are also unresolved issues about catalyst deactivation at low temperature, sulfur resistance or Pt site/state role during lean and rich phase, as well as CO competitive adsorption over active centers [12,29,30]. Another crucial aspect for the NSR technology constitutes soot formation and its presence in the system during both lean and rich steps [6,7,34,35].

For real-live application, it seems to be necessary to understand better the NSR mechanism under real conditions in order to improve the emission control, minimize fuel consumption and maximize catalyst efficiency. In the present work, the potential use of Pt–Ba/Al_2O_3 and Pt–K/Al_2O_3 as the NSR catalyst in the simultaneous removal of soot and NO_x has been studied. The detailed studies have been performed over soot-free catalysts, and the results are presented and discussed in comparison with the data obtained for catalyst + soot mixtures. This paper includes some explanation about soot influence on the catalysts' performance under cyclic reaction conditions.

* Corresponding author. Fax: +34 952131919.
E-mail address: luijo@uma.es (L.J. Alemany).

0021-9517/$ - see front matter © 2010 Elsevier Inc. All rights reserved.
doi:10.1016/j.jcat.2010.01.003

2. Experimental

2.1. Catalyst preparation and characterization

In the present work, the following catalysts were used 0.4Pt/γ-Al_2O_3, 4Ba/γ-Al_2O_3, 16K/γ-Al_2O_3, 0.4Pt–4Ba/γ-Al_2O_3 and 0.4Pt–16K/γ-Al_2O_3, denoted further as 0.4Pt, 4Ba, 16K, Pt–Ba and Pt–K, respectively. The metal loading is expressed as formal surface atomic density (atoms per nanometer square, at/nm^2). The catalyst formulations are summarized in Table 1. All catalysts were prepared by incipient wetness impregnation. First, the Pt/γ-Al_2O_3 monometallic catalyst was obtained after impregnation of the γ-Al_2O_3 support (Sasol, PuraloxCa, A_{BET} = 200 m^2/g and V_p = 0.7 cm^3/g) with an aqueous solution of diamminedinitroplatinum (II) ($Pt(NH_3)_2(NO_2)_2$, Aldrich), drying overnight at room temperature and calcination for 3 h at 648 K in air. Then, Ba or K was introduced as aqueous solutions of barium acetate ($Ba(CH_3COO)_2$, MERCK) or potassium acetate (CH_3COOK, Riedel de Haën) to Pt/γ-Al_2O_3 to obtain bimetallic Pt–Ba or Pt–K catalyst, respectively. The final calcination was performed during 5 h at 798 K in air.

The 4Ba/γ-Al_2O_3 and 16K/γ-Al_2O_3 catalysts were obtained by impregnation of γ-Al_2O_3 with aqueous solution of Ba and K, respectively, drying overnight at room temperature and calcination for 5 h at 798 K in air.

Printex U (Degussa, A_{BET} = 97 m^2/g) was used as a model soot. The composition of soot via elemental analysis technique (Elemental Analyser LECO CHNS 932) was found as 97.17, 1.16, 0.19 and 0.31 wt.% of C, H, N and S, respectively (ash was not detected). The detailed properties of Printex U are well described in the literature [36,37]. To obtain a soot + catalyst mixture, the desired amount of soot was added to the previous prepared catalyst in the presence of H_2O (powder to water ratio was 2000:1 wt.). Next, sample has been mixed for 1 h and dried during 24 h at 363 K. This procedure was used to prepare the Pt/γ-Al_2O_3 + soot (Pt + soot), Ba/γ-Al_2O_3 + soot (Ba + soot), K/γ-Al_2O_3 + soot (K + soot), Pt–Ba/γ-Al_2O_3 + soot (Pt–Ba + soot), Pt–K/γ-Al_2O_3 + soot (Pt–K + soot), γ-Al_2O_3 + soot (Al + soot). The soot content in each sample was 10 wt.%. For diffuse reflectance infrared Fourier transform spectroscopy (DRIFTS) study, the catalysts + soot mixtures with soot content of 1 wt.% were prepared as described earlier.

Soot-free catalysts as well as catalyst + soot mixtures before and after soot combustion experiments were characterized by Transmission Electron Microscopy (TEM), X-ray Diffraction (XRD) and X-ray Photoelectron Spectroscopy (XPS).

The TEM images were taken with a Philips CM200 (200 kV) microscope equipped with an EDX (Energy Dispersive X-ray) detector on powder samples deposited onto a copper mesh grid coated with a carbon film.

The XRD patterns of the powder samples were recorded with a Siemens D-501 goniometer equipped with a Johansson type primarily monochromator with a Ge(1 1 1) crystal. During measurement, Cu $K_{\alpha1}$ radiation and a fixed power source (45 kV and 35 mA) were used.

The XPS spectra were obtained by using a Physical Electronic 5700 spectrometer with Mg K_α X-ray source and hemispherical electron analyzer. The carbon C 1s peak at 284.8 eV was used as internal standard for determining peak positions within ±0.2 eV accuracy. All deconvolutions of experimental curves were done with Gaussian–Lorenzian line fitting of varying proportions (60–80%).

Table 1
Formulation of studied catalysts.

Catalyst	Pt (wt.%)	Ba (wt.%)	K (wt.%)	Al_2O_3 (wt.%)
γ-Al_2O_3	–	–	–	100
0.4Pt/γ-Al_2O_3	2	–	–	98
4Ba/γ-Al_2O_3	–	20	–	80
16K/γ-Al_2O_3	–	–	20	80
0.4Pt–4Ba/γ-Al_2O_3	2	20	–	78
0.4Pt–16K/γ-Al_2O_3	2	–	20	78

2.2. Catalytic study

2.2.1. Soot combustion

The O_2-assisted (3% of O_2 in He flow) and NO_x-assisted (1000 ppm of NO + 3% of O_2 in He flow) soot combustion has been performed for catalyst + soot mixtures in the temperature range 273–1073 K. The temperature ramp was 10 K min^{-1}. The reactions were carried out in a quartz flow-reactor with fixed bed. The outlet gasses were analyzed by a quadruple mass spectrometer QMS 200 (Pfeiffer Vacuum Prisma™). The temperature was controlled by a PID-TIC1 controller equipped with a K-type thermocouple. The 40 mg of the catalyst + soot powder and the total flow of the gases 40 ml min^{-1} were used for each combustion test (GHSV = 2.8 × 10^4 h^{-1}, at 1 atm and 293 K).

2.2.2. Transient response method (TRM)

TRM runs were performed in quartz tube reactor connected to the QMS 200 mass spectrometer. The method was applied to study the NO_x storage–reduction process over soot-free catalysts. Experiments were carried out at a constant temperature of 623 K under the total gas flow 100 ml min^{-1} using 60 mg of catalyst (GHSV = 10^5 h^{-1}, at 1 atm and 293 K). A rectangular pulse of NO (1000 ppm) + O_2 (3%) in He flow and H_2 (2000 ppm) in He flow were subsequently fed during the oxidation and reduction step, respectively. The NO_x adsorption–reduction periods were separated by a He purge (time of purge was approximately 30 min). The reductant/oxidant ratio was kept as 2 for all reactions. For all experiments, the *N*-balance was closed with deviation 3–5%.

2.2.3. In situ DRIFTS–TRM

The simultaneous soot combustion and NO_x removal were studied under TRM lean-rich cyclic conditions without He purge between steps. The reaction was performed in a continuous flow DRIFT Harrick Praying Mantis™ reaction chamber connected to the QMS 200 mass spectrometer. FTIR Nicolet Nexus 6700 spectrometer was applied to study in situ the catalysts surface performance during the experiment, whereas outlet gas was analyzed by MS. The studies were performed for the soot-free catalysts and catalyst + soot mixtures. Before experiments, He flow (1 h, flow 25 ml min^{-1}, GHSV = 1.8 × 10^4 h^{-1}) was applied to clean the chamber and the experimental line. The reactions were carried out at a constant temperature of 623 K. The accumulation step (1000 ppm of NO + 3% of O_2 in He flow, 15 min) was directly followed by the regeneration step (2000 ppm of H_2 in He flow, 15 min). The temperature was adjusted and controlled by the Harrick ATC low voltage controller with a K-type thermocouple. Spectra were recorded in diffuse reflectance mode (DRIFT), and 64 scans were collected at resolution 1 cm^{-1}.

3. Results and discussion

3.1. Catalysts characterization

The specific surface area (A_{BET}), given by Sasol, for the pure γ-Al_2O_3 support was 200 m^2/g. After impregnation and calcination, the A_{BET} of the Pt–Ba/Al_2O_3 and Pt–K/Al_2O_3 catalysts decreased around 10–30% comparing to this of the fresh support. The decrease in the A_{BET} was higher for the Ba-bearing than that for the

K-bearing catalyst, which has also been shown elsewhere for the NSR catalyst standard formulation (1:20:100) [6].

TEM images of the Pt–Ba + soot and Pt–K + soot catalyst before soot combustion are presented in Fig. 1a and b, respectively. Fig. 1a′, a″ and b′, b″ shows the Pt–Ba + soot and Pt–K + soot catalyst after soot combustion, respectively. Both for Pt–Ba + soot (Fig. 1a) and Pt–K + soot (Fig. 1b), at least two types of crystallites are observed. One of them possesses a round-like shape and large thickness, corresponding to alumina containing Pt (the presence of Pt was also detected by EDX analysis performed during the TEM study). The second type of crystallites has a needle-like structure and was assigned to the Ba- or K-carbonate phase. After O_2-assisted (Fig. 1a′ and b′) and NO_x-assisted (Fig. 1a″ and b″) soot combustion, both of the catalysts showed significant textural and morphological changes.

For all prepared material, Pt forms rather small spherical particles. Average Pt size diameter was ca. 8 and 15 nm for samples before and after reaction, respectively. In the case of Pt–K system, TEM images (Fig. 1b, b′ and b″) exhibit that potassium can form melt-like structure, which stick to the catalyst surface masking Pt sites. To obtain the Pt–K system, 16 atoms of K per nm^2 of Al_2O_3 were introduced during the impregnation. This amount of K corresponds to ca. 20 wt.% of the metal loading and gives more than a monolayer. Based on previous study [29,30], the accumulation capacity of such prepared Pt–K catalyst is comparable with the accumulation capacity of the Pt–Ba catalyst. It implies that both the catalyst surface and Pt particle coverage by alkali element occurs in higher extent for Pt–K than that for the Pt–Ba catalyst. Therefore, the amount of Pt accessible for conventional dispersion measurement can be affected. FTIR analyses via CO adsorption at low temperature for the Pt and Pt–Ba catalysts (data not presented here) exhibited the presence of bands at 2090, 2160, 2185 and 2280 cm^{-1}, which can be attributed to the different Pt sites [38,39]. These bands were also observed for K-based catalyst; however, these bands were far weaker and disappear at temperatures higher than 143 K. The dispersion of Pt, estimated from CO adsorption, was ca. 45% and 30% for the Pt–Ba and Pt–K systems, respectively. Good dispersion of Pt implies a proximity of the Pt sites to alkali metal which constitutes potential nitrates storage [5]. In accordance with the broad accepted storage model, i.e., nitrites/nitrates route, [25,40–44] nitrites are progressively transformed into barium nitrates on $NO + O_2$ admission with Pt participation [43]. The same behavior was observed for the Pt–Ca/Al_2O_3 catalyst at 573 K [41], BaO/Al_2O_3 and Pt–BaO/Al_2O_3 catalysts [44]. Small Pt particles can be beneficial for NO to NO_2 oxidation and through this facilitate NO_x accumulation. However, too high Pt dispersion is not desirable for NSR reaction. Smaller Pt crystallites can be easier oxidized than bigger ones in the presence of O_2, or via net oxidation [23].

The XRD pattern of the Pt–Ba + soot and Pt–K + soot catalyst before (BR) and after (AR) soot combustion in NO_x are presented in Fig. 2a and b, respectively. The characteristic structure for γ-alumina (JCPDS 75-0921), Pt and PtO (JCPDS 4-0802 and JCPDS 83-1997) and graphite (JCPDS 46-0943) is observed for both Ba- and K-based systems. For the Pt–Ba + soot catalyst (Fig. 2a), Witherite ($BaCO_3$ JCPDS 5-0378) was a Ba-dominant phase in sample both before (BR) and after soot combustion experiment (AR). For the Pt–K + soot system before soot combustion (pattern Pt–$K_{(BR)}$ in Fig. 2b), obtained data evidenced the presence of potassium carbonate phase, mostly $K_4H_2(CO_3)_3{\cdot}1.5H_2O$ (JCPDS 20-0886). The potassium carbonate phase in the Pt–K + $soot_{(BR)}$, sample was accompanied by the K_2O phase (JCPDS 43-1020). After reaction (pattern Pt–K + $soot_{(AR)}$ in Fig. 2b), potassium phases were detected in some extent. However, as indicated by TEM study, K tends to form such a melt-like structure, which was probably difficult to measure by XRD or was considered in low 2θ region of the XRD pattern. The comparison of XRD patterns of catalysts before (BR) and after reaction (AR) suggests that the recrystallization process

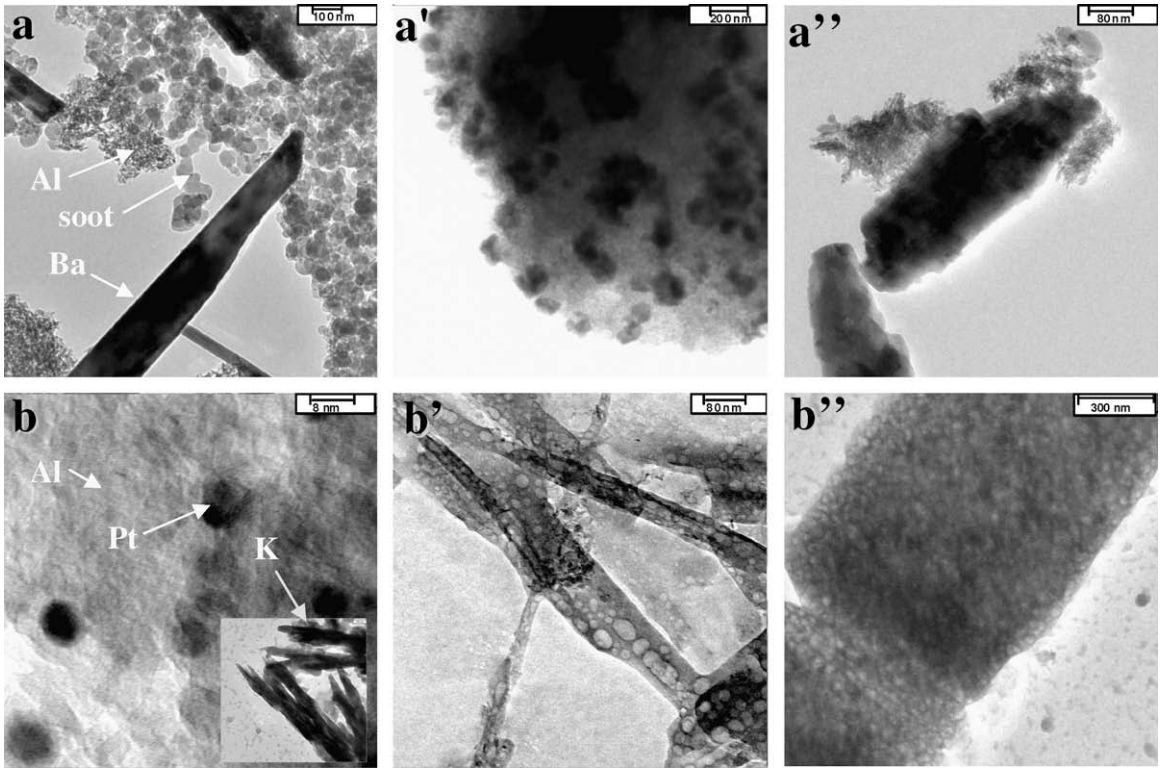

Fig. 1. TEM images of (a) Pt–Ba + soot and (b) Pt–K + soot (soot content 10 wt.%) before and after soot oxidation in (a′ and b′) oxygen (3% of O_2 in He flow) and (a″ and b″) NO_x (1000 ppm of NO_x + 3% of O_2 in He flow). Total flow rate 40 ml min^{-1} T range 298–1073 K.

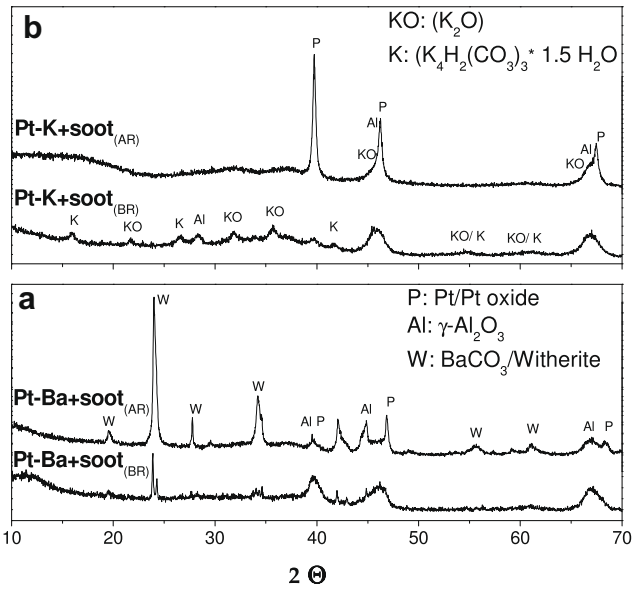

Fig. 2. XRD patterns of (a) Pt–Ba + soot and (b) Pt–K + soot catalysts before (BR) and after (AR) soot combustion in NO_x under total flow 40 ml min^{-1} (1000 ppm of NO_x + 3% of O_2 in He), *T* range 298–1073 K.

occurs during soot oxidation in the temperature range 298–1073 K. For both of the systems, signals arising from Pt were better defined in catalysts after soot combustion suggesting higher crystallite order in the samples. The Ba carbonate phase is also well defined as demonstrated by corresponding 2θ signals ($BaCO_3$ JCPDS 5-0378). In contrary, for the Pt–$K_{(AR)}$ system, the signals arising from K-carbonate phase are very weak and additionally a broad peak at low 2θ is detected. It suggests the melt-like structure, mentioned previously, or very small K particles are formed. This can support our previous statement that indeed some Pt species can be covered by K phase. Because of that they can be not or hardly accessible for reactants during combined NO_x–soot removal, at least at primary stage of this process.

In Table 2, the XPS data of Pt $4d_{5/2}$ region are presented for the Pt–Ba + soot and Pt–K + soot catalysts both before (BR) as well as after NO_x-assisted soot combustion (AR). XPS reveals the rearrangement of platinum and alkali components in the catalysts after soot combustion. During oxidation, soot was removed from the catalysts surface, up to ca. 80% for both Ba- and K-based catalyst, which affects atomic concentrations. The Al/Pt ratio was changed from 12 to 28 for Pt–Ba + soot and from 8.5 to 11 for Pt–K + soot before and after reaction, respectively. This Al/Pt ratio for both catalysts was determined from multiplying by corresponding atomic sensitivities factors (ASF) the relative integrated intensities of the respective Al 2p and Pt 4d core level spectra (not shown). For the Pt–Ba + $soot_{(BR)}$ and Pt–K + $soot_{(BR)}$ catalysts, the binding energies (E_B) of Pt^0 (Table 2) are comparable, and observed differences were found in error range (±0.2 eV). The E_B values of Pt^0 are shifted to higher energy for catalysts after soot combustion. The value of E_B shift is comparable for both Pt–Ba + soot and Pt–K + soot systems, i.e., 0.7 eV and 0.6 eV, respectively. It may suggest that during soot combustion, the electron density was modified causing that Pt sites on catalysts surfaces become more positive. Moreover, XPS study demonstrates that Pt oxidation state changed during the reaction. For the Pt–K + $soot_{(AR)}$ catalyst, the Pt^0/Pt_{ox} ratio was changed from 0.72 to 0.26, while it was almost not influenced in the Pt–Ba + soot systems. The value of ca. 0.70 is roughly constant for samples before and after reaction. Preliminary study showed that the Pt oxidation state is affected by alkali element. The Pt^{4+} formation was preferred for the Pt–K catalyst, while for Pt–Ba–Pt^{2+}. The Pt oxidation state on catalyst surface is of importance when the dual function of the catalyst, i.e. NO_x storage and soot removal, is taken into account. From that point of view, the *good cooperation* between alkali element and Pt is desirable [7,45,46]. This *good cooperation* means the stabilization of Pt^0 and the maintenance of a constant Pt^0/Pt_{ox} ratio during all NO_x–soot removal process. Presented XPS data suggest that better Pt–alkali component cooperation was achieved in the case of the Pt–Ba catalyst.

Table 2
XPS data of Pt $4d_{5/2}$ region for Pt–Ba and Pt–K catalyst before (BR) and after soot oxidation (AR) with $NO_x + O_2$ under total flow rate 40 ml min^{-1} (1000 ppm of NO_x + 3% of O_2 in He flow).

	$Pt4d_{5/2}$ E_B (eV ± 0.2)	
	Pt–Ba/γ-Al_2O_3	Pt–K/γ-Al_2O_3
Pt^0	313.7 $(43)_{BR}$ 314.4 $(39)_{AR}$	313.5 $(42)_{BR}$ 314.1 $(21)_{AR}$
Pt_{ox}	317.2 $(57)_{BR}$ 317.1 $(61)_{AR}$	317.4 $(58)_{BR}$ 317.2 $(79)_{AR}$

(%) species concentration, P_{ox} = PtO + PtO_2.

3.2. Catalytic study

3.2.1. Soot combustion

Figs. 3 and 4 show MS spectra of soot combustion for the Pt–Ba + soot and Pt–K + soot catalysts in the presence of O_2 and NO_x, respectively. During soot oxidation only CO_2 and H_2O were produced over the catalysts, and no significant level of CO was detected, except the soot, Al + soot and Ba + soot systems, in which CO formation was observed in amounts higher than 60 ppm above 723 K. Therefore, only CO_2 (panel a in Figs. 3 and 4) and H_2O (panel b in Figs. 3 and 4) profiles are presented.

The temperature of soot ignition (T_{ign}) in the presence of O_2 (Fig. 3) was 673 K and 573 K for the Pt–Ba + soot and Pt–K + soot, respectively. The T_{ign} value over monometallic Pt + soot catalyst and Al + soot were almost the same, i.e., ca. 700 K, and equal to T_{ign} of pure soot. During O_2-assisted soot combustion (Fig. 3), the largest amounts of CO_2 and H_2O was formed over the Pt–K + soot catalyst, i.e., 25,600 ppm at 923 K and 19,680 ppm at 723 K, respectively. The amount of CO_2 produced during soot combustion gradually decreased for the studied materials in the following order Pt–K > 16K > Pt–Ba > Pt > 4Ba > Al_2O_3 > pure soot. The differences in H_2O production between Pt–K + soot, Pt–Ba + soot, Pt + soot and Al + soot were in the range from 40 to 49%. For pure soot, H_2O was not detected up to ca. 900 K.

In Fig. 4, the results of NO_x-assisted soot combustion are shown. The temperatures of soot ignition in the presence of NO_x were lower about 50 K than that observed for soot ignition in the presence of O_2. The total amount of CO_2 produced during soot combustion follows the order Pt–K > 16K > Pt–Ba > Pt > 4Ba > Al_2O_3 > pure soot. CO_2 and H_2O profiles obtained for both experimental conditions suggest that alkali element has an influence on the soot ignition temperature as well as on the combustion profile. The T_{ign} of soot was lower ca. 100 K for the Pt–K catalyst comparing to T_{ign} characteristic for ignition of soot over the Pt–Ba catalyst. Moreover, the ignition of soot seems to be connected with water release from the samples. Fig. 3a shows that all CO_2 lines followed directly H_2O perturbations. However, main soot combustion took place at temperatures higher than 700 K. For all reaction conditions studied (Figs. 3 and 4a), K modified the combustion temperature as well as divided soot oxidation into a few steps. The CO_2 profiles obtained during soot combustion over Pt–K show three peaks instead of one, as was observed for the Pt–Ba + soot catalysts (Figs. 3 and 4a). Additionally, the alkali metal affected the soot oxidation rate.

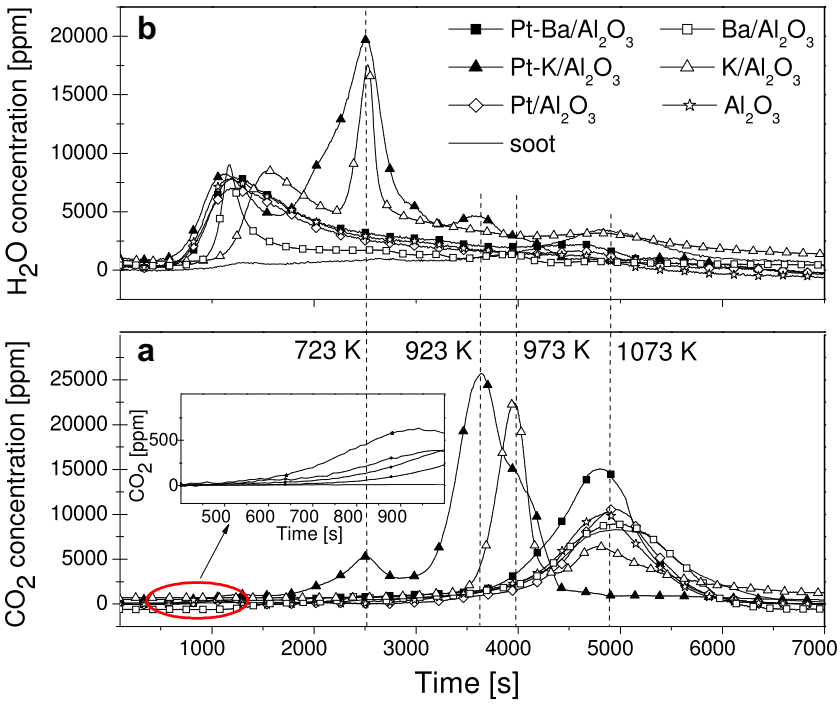

Fig. 3. MS profiles of (a) CO_2 and (b) H_2O for soot oxidation in O_2, total flow 40 ml min^{-1} (3% of O_2 in He), T range 323–1073 K, ramp 10 K min^{-1}.

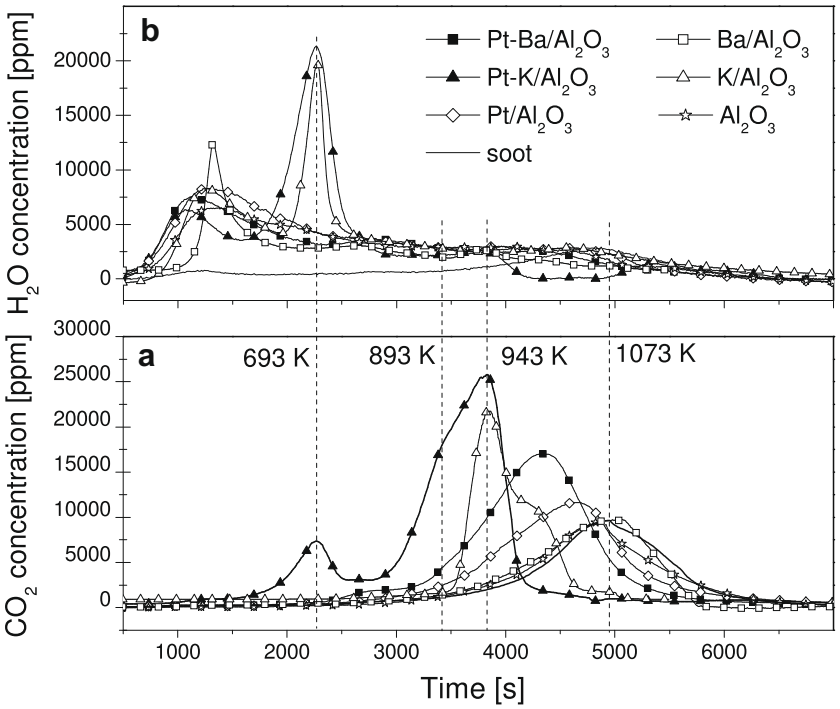

Fig. 4. MS profiles of (a) CO_2 and (b) H_2O for soot oxidation in NO_x, total flow 40 ml min^{-1} (1000 ppm of NO_x + 3% of O_2 in He), T range 323–1073 K, ramp 10 K min^{-1}.

In the case of the Ba-containing sample, after ignition rather slow soot oxidation was observed (Fig. 3a), whereas the Pt–K catalyst showed rapid soot oxidation after ignition.

Soot combustion experiment revealed that all catalysts were able to oxidize soot in oxygen flow in the absence and presence of NO_x. It is important to note that in the present work, a model soot Printex U was used. According to the previous studies [36,37], there is a certain difference between this model soot and realistic soot that is normally produced in the real-life Diesel engine operation. The content of adsorbed hydrocarbon in the Diesel soot is greater comparing to that in Printex U what clearly affects its reactivity to O_2 [37]. The less quantity of hydrocarbons in Printex U explains its less reactivity to O_2. The reactivity of soot is higher in NO_x atmosphere than in O_2 and can be further enhanced along with selectivity toward N_2 and CO_2 by the catalyst usage [36]. The data reveal the beneficial effect of the K-containing catalyst on soot

combustion when comparing with Ba-based system. This is in line with the literature data for the Pt–K catalyst [6] and Pt–K modified by Mn [5]. Previous studies [6,47,48] explain the behavior of lowering the T_{ign} of soot for the Pt–K system by the promoting effect of K. In fact, an increase in the catalytic activity in terms of soot combustion could be noticed for 16K and Pt–K; therefore, obtained results can support the statement that K promotes soot combustion. This promotion can be connected with the properties of K compounds present on the catalyst surface [47] and also with the presence of —OH group. It has been found that water facilitates soot combustion [49,50]. A significant promotion of the soot combustion rate over perovskite-type mixed oxides was observed when 10% of water was added into the reactant gas. The study of soot oxidation in a flow-reactor [49] reveals that when NO_2 exists with O_2 and H_2O, the reaction rate increases in proportion to NO_2. The oxidation rate increases nonlinearly with O_2 or H_2O concentration when the other two oxidants are fixed. The activation energy for Printex U oxidation with NO_2–O_2–H_2O was determined [49] to be 40 ± 2 kJ/mol, with the first order of carbon in the range of 10–90% oxidation and in the temperature range of 523–723 K. This value was lower than the activation energy of NO_2–O_2 oxidation, which was 60 ± 3 kJ/mol. The interaction of soot particles with water has been described [51–55] according to their hydrophobic and hydrophilic properties. Probably, retained water improves the contact between soot and catalyst active site and thus facilitates soot combustion. Moreover, the activation of carbon black by water was proposed [50] through a water–gas reaction formulated as $C + H_2O \rightarrow CO + H_2$ or subsequent water–gas-shift (WGS) reaction formulated as $CO + H_2O \rightarrow CO_2 + H_2$, which might also take place, resulting in an obvious acceleration in the combustion rate.

The mechanism of soot oxidation with and without catalyst has been extensively studied [3,14,50,56–63]. A possible mechanism for this reaction, involving oxygen as oxidant, is dissociative chemisorption of oxygen, leading to oxygen radicals that subsequently form (unstable) surface oxygen complexes that subsequently will decompose forming CO and CO_2 [14]. This was primarily proposed for non-catalytic soot oxidation [60,61,64,65], and later it was suggested that the mechanism of the metal-catalyzed reaction can be similar to the non-catalytic reaction [14]. This mechanism provides for both CO and CO_2 formation as primary products, where under non-catalytic condition the CO/CO_2 ratio is dependent on the oxygen supply and temperature [45]. The mechanism of soot oxidation in different oxidizing atmosphere was also proposed [63]. This mechanism bases on surfaces oxygen complexes (SOCs) formation as soot oxidation intermediates. When NO_2 is present together with O_2 in the gas mixture, the oxygenated carbon complexes were firstly formed from the reaction of Printex U with NO_2 [63]. The same effect was observed for reaction with NO and O_2 mixture over the Pt-based catalyst. The soot combustion study over the alkaline and the alkaline-earth oxide catalysts [45] suggests the formation of the alkaline oxygenated compounds which play role during oxygen transfer process. According to this indication, an increase in the catalytic activity with the electropositivity of the alkali metal was shown [45]. However, the electropositivity effect of alkali element can be expected in full contact with soot [45]. It was suggested [45] that in loose system, this effect is no more observed, and the reactivity of alkali-species is limited by the efficiency of the contact between soot and the active sites [45] what is in line with previous study [62,66]. In addition, the formation of surface –OH groups or chemisorbed water was found to promote the elimination of soot [50] what was mentioned earlier.

The high activity in the soot combustion of the K-containing samples (lose contact) was observed (Figs. 3 and 4). This behavior was attributed to the volatile nature of possible oxides, peroxides of K or trace nitrates present on the catalyst surface [47]. The mobility of such compounds is expected to be high, leading to the decrease in soot oxidation temperature. Moreover, Pt enhances the migration of such active species responsible for soot oxidation at much lower temperature compared with the K–Al_2O_3 catalyst alone. It has also been suggested that potassium can promote the formation of low melting point compounds that wet the soot surface, increasing its contact with the catalyst and thus improving activity [7]. Additionally, K is capable to easy adsorb water, which is formed during soot oxidation. The K migration, indicated by previous study [7,47], possibly provides both water presence and the proximity of the Pt and K species, whose synergetic effect was also reported [6,47,67]. This could be of importance during simultaneous NO_x–soot removal process over the NSR catalyst, where during the lean phase of TRM, soot removal takes place similar as in the case of NO_x-assisted soot combustion. The decrease in the soot ignition temperature in the presence of NO_x (lean phase) can be associated with the NO_x conversion to NO_2, which then reacts with soot and increases the soot oxidation rate. Under reduction condition (rich phase of TRM), direct H_2O formation usually occurs [23]. In general, during rich phase, soot removal can be performed by NO_2, which is a product of partial nitrites/nitrates reduction [45,68]. Considering obtained results, this removal can be accelerated by water and can give the CO or CO_2 peak at the primary stage of rich phase, when CO_2 concentration is higher than storage capacity of alkali or alkaline-earth metal. The rapid oxidation may evoke an increase in the local temperature, which is not desired for the catalyst. The recent study of Li et al. [48] reports that the alkali component is responsible for the enhancement of the catalyst–soot surface lattice oxygen transfer. This effect, however, is expected in a tight contact of the catalyst with soot where the lattice oxygen is quickly replaced by oxygen from the gas phase. During the performed study, rather a loose contact between soot and catalysts was obtained (the contact between soot in Diesel Oxidation Catalyst DOC in realistic condition is loose). Because of the loose contact between soot and catalyst, the effect of the monometallic catalyst (Pt/Al_2O_3) on the soot combustion is not observed comparing with soot combustion over alumina or with pure soot combustion without catalyst participation.

3.2.2. Transient response method

The NO_x storage–reduction over the Pt–Ba and Pt–K soot-free catalysts has been studied at 623 K, and the obtained results are shown in Figs. 5 and 6, respectively. The lean-rich cycles have been obtained after conditioning the catalyst at the same temperature with 4–5 adsorption–reduction cycles, until a stable catalyst behavior was obtained. The NO, NO_2 and NO_x ($NO_x = NO + NO_2$) outlet concentrations were plotted in function of time along with NO inlet concentration. For Pt–Ba during lean phase (Fig. 5a) and upon NO admission to the reactor at $t = 0$ s, the dead time in NO outlet concentration was observed, indicating that NO_x was stored on the catalyst surface. After ca. 40 s, the NO outlet concentration gradually increased with the time, reaching ultimately the inlet concentration value of 1000 ppm at the end of the phase at 1500 s. The corresponding NO_2 evolution (NO_2 line in Fig. 5a) was observed demonstrating the oxidation of NO to NO_2 over Pt sites. The NO_2 concentration reached 250 ppm at 1500 s. The CO_2 signal was not observed during this step, suggesting that $BaCO_3$ phase was fully decomposed during conditioning, leaving on the surface BaO and $Ba(OH)_2$. The amount of stored nitrates was 1.237×10^{-3} mol/g_{cat}. This value was estimated taking into account that the amount of stored nitrates is proportional to the area A_1 in Fig. 5a (Fig. 6a for Pt–K catalyst). In Fig. 5b, the reduction of stored nitrates/nitrites with H_2 at 623 K is presented for Pt–Ba. Upon H_2 admission to the reactor at $t = 0$ s, H_2 was completely consumed for about 180 s. Then, the H_2 outlet concentration gradually

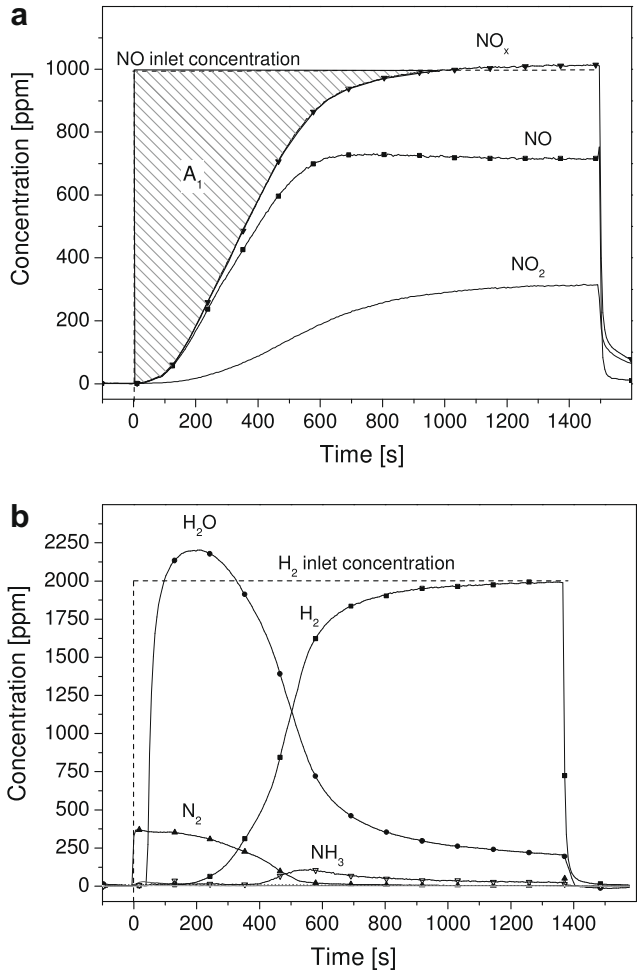

Fig. 5. TRM profile for the Pt–Ba catalyst at 623 K (a) lean phase (1000 ppm of NO_x + 3% of O_2 in He) and (b) rich phase (2000 ppm of H_2 in He). Total flow 100 ml min^{-1}.

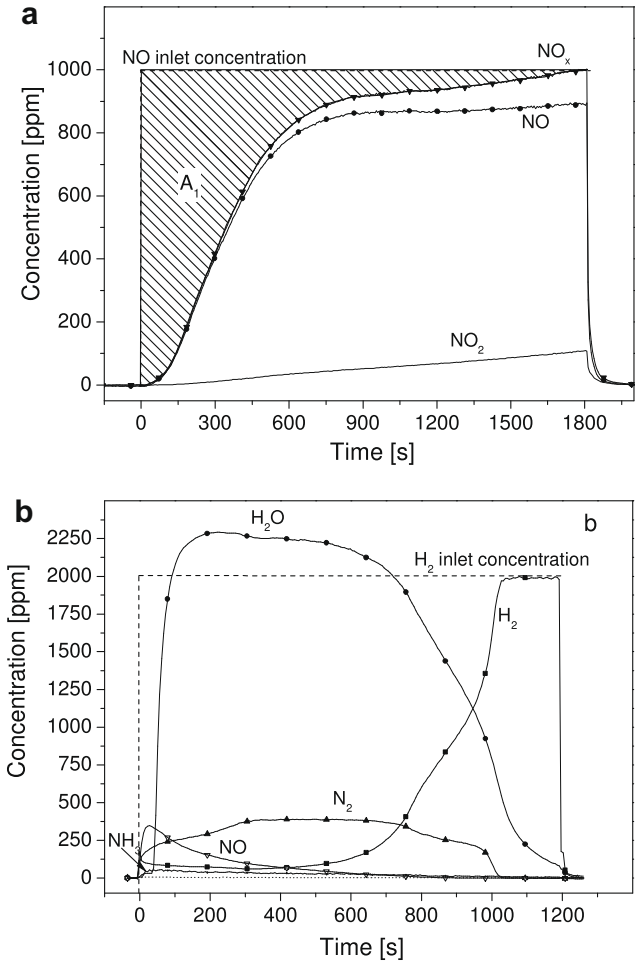

Fig. 6. TRM profile for the Pt–K catalyst at 623 K (a) lean phase (1000 ppm of NO_x + 3% of O_2 in He), (b) rich phase (2000 ppm of H_2 in He). Total flow 100 ml min^{-1}.

increased with the time, restoring inlet value at the end of rich step at ca. 1400 s. N_2 was directly formed, suggesting a fast reduction of stored nitrites/nitrates. After 350 s, while N_2 and H_2O concentration decreased and H_2 approached inlet concentration, NH_3 was observed in amount ca. 100 ppm.

In Fig. 6a and b, the typical data obtained during storage–reduction cycles over the Pt–K soot-free catalyst are presented. The collected data for lean phase (Fig. 6a) were similar to these obtained for the Pt–Ba catalyst (Fig. 5a). Both NO and NO_2 were detected in reactor outlet gases with NO breakthrough observed for ca. 40 s. At the end of lean phase, at saturation point (1800 s), the NO_2 concentration value hardly reached 100 ppm, pointing out that the NO to NO_2 oxidation capacity is lower for Pt–K than that for Pt–Ba. This effect can be explained by high content of K. If the K content is high, what takes place in the case of the Pt–K system with 16 atoms of K per nm^2, then the catalyst surface is fully covered and the oxidation capacity of Pt/Al_2O_3 is no longer available or available, but in less extent than in the case of Pt–Ba. The amount of stored nitrates 1.236×10^{-3} mol/g_{cat} was similar to that evaluated for the Pt–Ba catalyst. The CO_2 signal was not observed during lean phase, suggesting that K was present on the catalyst surface mostly as KOH or K_2O. MS profiles obtained for the reduction of stored nitrates/nitrites with H_2 over Pt–K (Fig. 6b) were different comparing to these obtained for reduction step over Pt–Ba (Fig. 5b). Upon H_2 admission to the reactor at $t = 0$ s, complete H_2 consumption was observed for about 500 s. The NO slip was detected at the beginning of rich step, indicating that the nitrites/nitrates reduction is less selective over Pt–K comparing to the Pt–Ba catalyst. The formation of N_2 took place during almost all reduction phase, supporting our statement that cooperation between Pt and K is not as efficient as in Pt–Ba system. The amount of NH_3 formed was negligible, and appears, if any, only at the beginning of the reduction phase.

In Fig. 7a and b, the sets of NO_x storage (15 min)–reduction (15 min) cycles at 623 K over the Pt–Ba + soot and Pt–K + soot catalysts (soot content 1 wt.%) are presented, respectively. The data evidenced the different behavior of the Pt–Ba and Pt–K catalysts during the simultaneous NO_x and soot removal. For the Pt–Ba + soot system (Fig. 7a) during first 6 lean cycles, soot was extensively removed giving CO_2 as a product. At the same time, the NO_x storage and concentration of NO_2 (lean phase) increased gradually with time, suggesting that CO_2 and NO/NO_2 competed for the same adsorption sites as was mentioned elsewhere [69]. From cycle 7, the catalyst performance was constant and highly reproducible up to 100 cycles (data not shown). For the Pt–K catalyst (Fig. 7b), soot oxidation was faster and during first 4 cycles most of the soot was removed. From cycle 1 to cycle 4, the NO_x storage gradually increased with time, but, in contrary to the Pt–Ba + soot (Fig. 7a) catalyst, for Pt–K + soot from cycle 5 (Fig. 7b), the deactivation was observed. The NO_2 concentration was similar for all cycles during the whole experiment. For rich phase, NO slip was not detected,

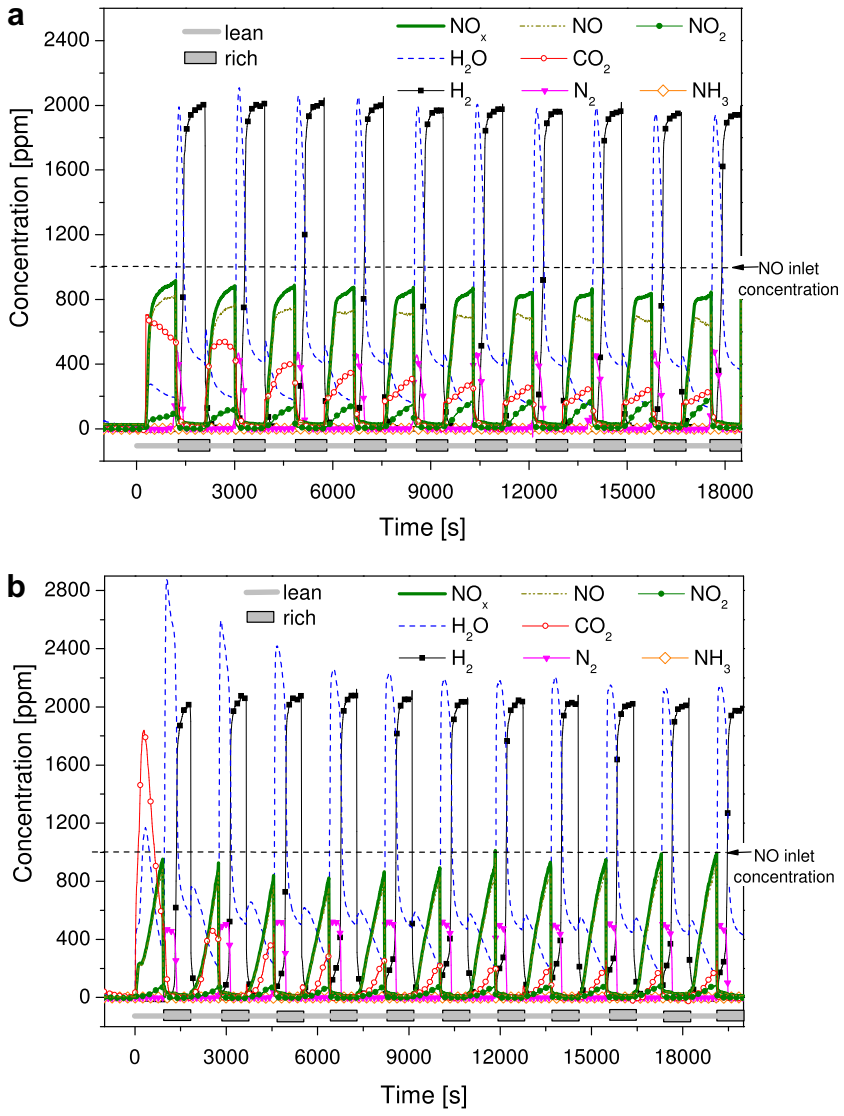

Fig. 7. Storage–reduction of NO_x at 623 K for (a) Pt–Ba + soot and (b) Pt–K + soot catalysts. Soot content 1 wt.%. Lean phase 15 min, 1000 ppm of NO_x + 3% of O_2 in He; regeneration step 15 min, 2000 ppm of H_2 in He. $NO_x = NO + NO_2$.

suggesting that the Pt–K + soot catalyst was more selective. For both the Pt–Ba + soot and Pt–K + soot catalyst, the amount of NH_3 formed during rich phase was negligible and stayed below 6 and 3 ppm, respectively.

In Fig. 8, the amount of NO_x stored and CO_2 produced over the Pt–Ba + soot and Pt–K + soot systems are plotted in function of cycle number. It can be noticed that CO_2 decreases the amount of NO_x accumulated, what can be assigned to competitive adsorption of CO_2 and NO_x over the storage component. The data reveal that the Pt–K catalyst was most efficient in terms of soot removal, but from cycle 5 lost progressively the NO_x accumulation capacity. In contrary, the Pt–Ba catalyst presented higher NO_x accumulation capacity, whereas the soot removal over this catalyst took longer time. From cycle 9, the amount of NO_x stored over Pt–Ba + soot was ca. 1.201×10^{-3} mol/g_{cat} and was similar to this evaluated for the Pt–Ba soot-free catalyst. At the same time, the amount of NO_x stored for the Pt–K + soot catalyst was 9.243×10^{-4} mol/g_{cat} and decreased in following cycles.

Fig. 9 shows NO_x conversion for the Pt–Ba and Pt–K soot-free and catalysts + soot mixtures. The Pt–Ba + soot mixture after 15 cycles was almost as efficient in NO_x removal as the Pt–Ba soot-free

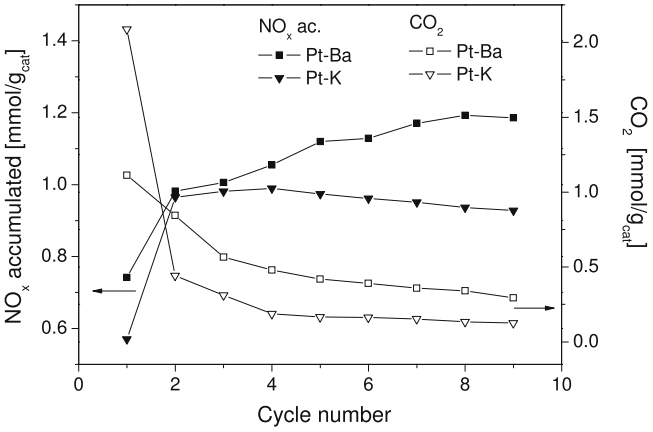

Fig. 8. The amount of NO_x stored and CO_2 produced in subsequent cycles upon simultaneous lean-rich cycling at 623 K over Pt–Ba + soot and Pt–K + soot catalysts. Soot content 1 wt.%. Lean phase 15 min 1000 ppm of NO_x + 3% of O2 in He; regeneration step 15 min, 2000 ppm of H_2 in He.

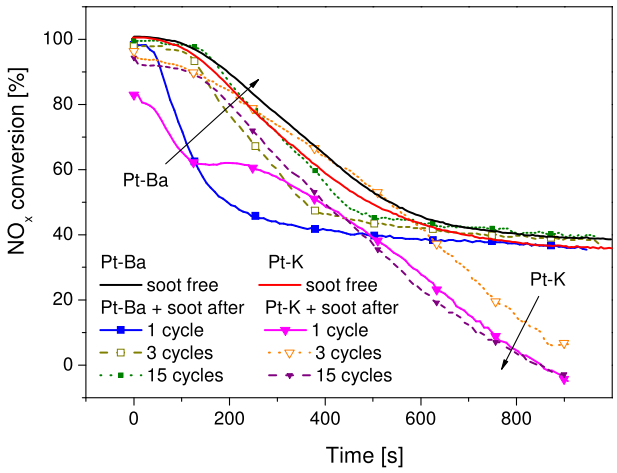

Fig. 9. NO_x conversions for the Pt–Ba and Pt–K soot-free catalysts and catalysts + soot mixtures for selected storage–reduction cycles.

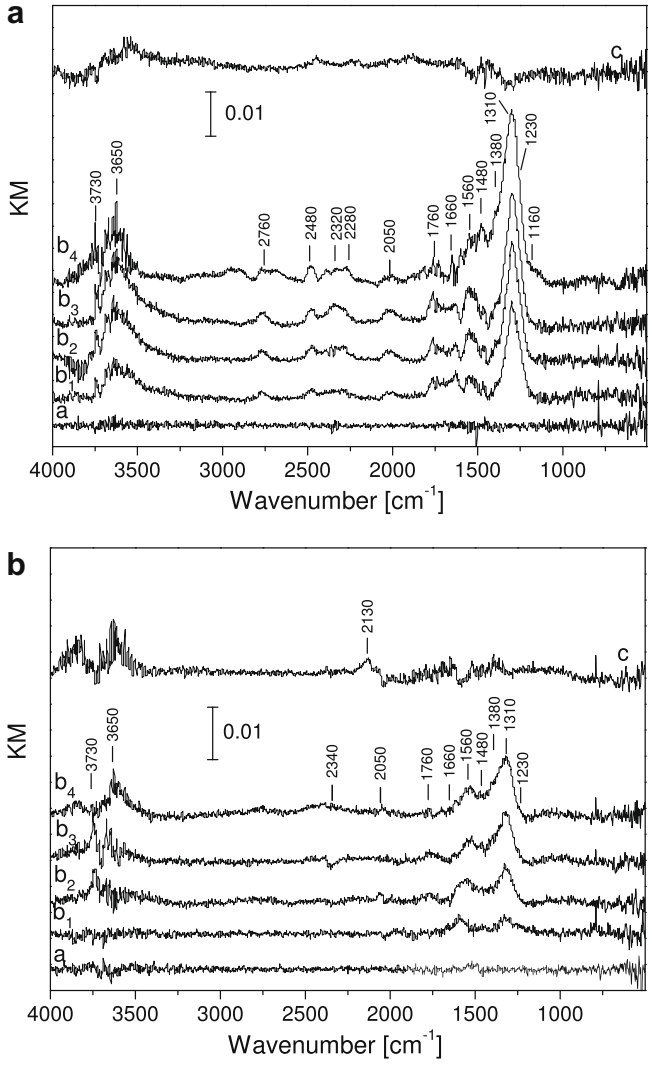

Fig. 10. DRIFT spectra recorded for storage–reduction cycles at 623 K over (A) Pt–Ba soot-free catalyst, (B) Pt–Ba + soot mixture (a) clean catalyst surface under He flow, (b) lean phase; nitrites/nitrates evolution under exposure to 1000 ppm of NO + 3% of O_2 in He (spectra recorded each 2 min), and (c) regeneration step with 2000 ppm H_2 in He. Soot content 1 wt.%. Total flow 25 ml min^{-1}.

catalyst, indicating that initial catalyst properties can be recovered with the time. In contrary, the NO_x conversion for Pt–K + soot was always below the NO_x conversion of the Pt–K soot-free catalyst, and with time the deactivation of catalyst was observed. For the Pt–K catalyst, the highest efficiency in NO_x removal was obtained in the 3rd cycle. However, this value consists of NO_x adsorption over K sites and NO_x participation in soot combustion. From cycle 4, the NO_x conversion of Pt–K + soot gradually decreased.

The obtained TRM data suggest that the alkali component has an influence on the general catalyst behavior during performed reaction. Pt–K presents better performance in terms of soot combustion; however, simultaneous soot and NO_x removal is performed with higher efficiency over the Pt–Ba catalyst. The physico-chemical catalyst characterization shows that Ba stabilizes Pt^0. The previous study pointed out the importance of the Pt–alkali component cooperation [7,45–47]. Importantly, the cooperation between Pt and alkali element (Ba or K), and also, as mentioned elsewhere [47], the properties, formation and mobility of nitrates/nitrites species can play a significant role during soot removal under cyclic lean-rich conditions. In rich phase, the oxidation of soot can take place with NO_2, which is a product of partial reduction of nitrites/nitrates stored over NSR catalyst. It suggests that the amount of NO_x stored over the catalyst in previous lean phase limits soot oxidation during rich step [47]. However, this process seems to be more complicated, and obtained data show also importance of (i) Pt–alkali metal cooperation, in particular, Pt^0/Pt_{ox} ratio stabilization by alkali component, (ii) H_2O formation and adsorption on catalyst surface species during combined NO_x–soot removal process, and (iii) CO_2 presence which displaced the $(NO/NO_2)_{ads} \Longleftrightarrow (NO/NO_2)_{gas}$ equilibrium. Therefore, the simultaneous NO_x and soot removal process will be affected by the sum of these three factors.

3.2.3. DRIFTS–TRM

Isothermal in situ DRIFTS–TRM (corresponding TRM profiles has been already discussed previously) for the soot-free catalyst and catalyst + soot mixtures are shown in Figs. 10A, 11A and 10B, 11B, respectively. Obtained results confirmed nitrites and nitrates species formation on the catalyst surface. A summary of the peak assignments used in this work is presented in Tables 3 and 4. On the surface of the Pt–Ba soot-free catalyst (Fig. 10A), the formation of nitrites and nitrates of various type (1100–1800 cm^{-1}) was observed under sample exposure to NO and O_2 at 623 K during the storage step (lines b in Fig. 10A). The peaks intensity increases with the contact time with NO + O_2 atmosphere. The formation of those features was also reported elsewhere for different catalysts formulations [20,27,42,68,70]. The band at ca. 1300 cm^{-1} can be assigned to the bidentate nitrites formation on highly dispersed Ba phase and/or on alumina support [68,70]. This band can be overlapped by band at 1310 cm^{-1}, which corresponds to bidentate nitrates formation [71,72]. The further vibrational mode of the bidentate nitrites species is observed at 1230 cm^{-1} together with a shoulder at 1160 cm^{-1}, which corresponds to bridged N-coordinated nitrites. Prolonged exposition of the Pt–Ba catalyst to NO + O_2 (lean phase) up to NO_x saturation (the saturation point was detected by MS) led to nitrites into nitrates transformation, and surface bidentate nitrates (bridging and/or chelating at 1650 and/or 1560 and 1310 cm^{-1}, respectively) and linear and/or unidentate nitrates (1480 and 1550 cm^{-1}) were formed [20,25,38,68,71,72]. This is with good agreement with previous data [44] where nitrites were observed to be the prevailing species at room temperature on the Ba/Al_2O_3 and $Pt–Ba/Al_2O_3$ systems, but above 473 K most of the nitrites were decomposed with formation of the corresponding nitrates. It is important to note that the formation of nitrates during NO + O_2 exposure requires the oxidation of adsorbed NO with reactive oxygen species that are present on the catalyst sur-

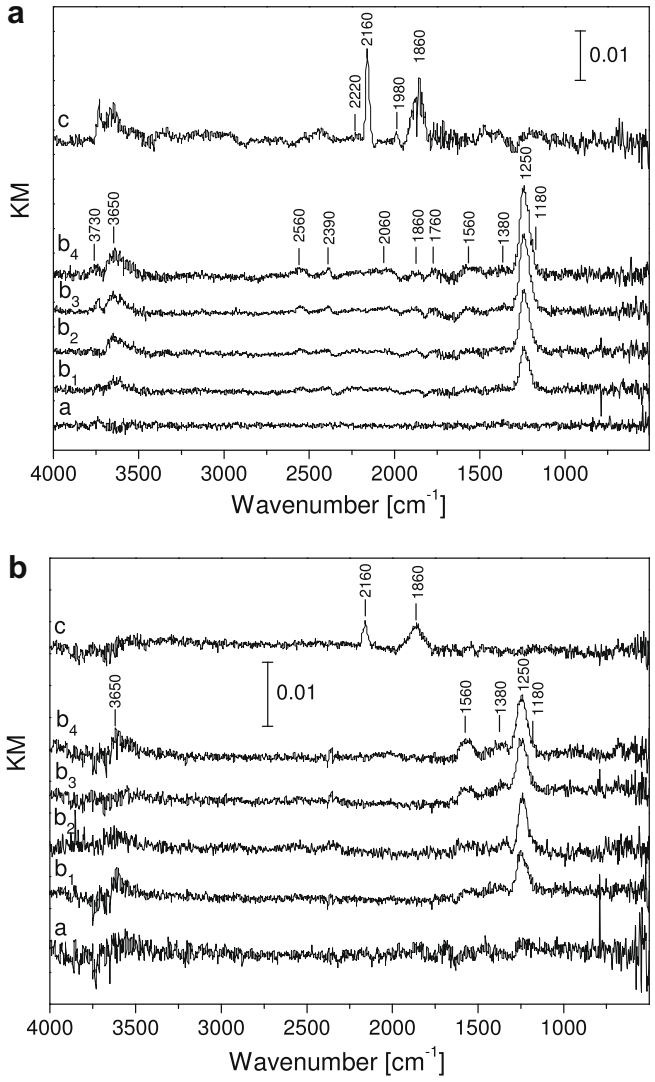

Fig. 11. DRIFT spectra recorded for storage–reduction cycles at 623 K over (A) Pt–K soot-free catalyst, (B) Pt–K + soot mixture (a) clean catalyst surface under He flow, (b) lean phase; nitrites/nitrates evolution under exposure to 1000 ppm of NO + 3% of O_2 in He (spectra recorded each 2 min), and (c) regeneration step with 2000 ppm H_2 in He. Soot content 1 wt.%. Total flow 25 ml min^{-1}.

Table 3
Assignments of peak position for Al-based adsorbates.

Wavenumber (cm^{-1})	Assignment	Ref.
1621–1610	Bridging bidentate nitrate, ν(N=O)	[70,72,73]
1260–1210	Bridging bidentate nitrate, $\nu(NO_{2as})$	
1590–1560	Chelating bidentate nitrate, ν(N=O)	[42,70,72,73]
1310–1290	Chelating bidentate nitrate, $\nu(NO_{2as})$	
1550	Unidentate nitrate, $\nu(NO_{2as})$	[38,72]
1257	Unidentate nitrate, $\nu(NO_{2asym})$	
1480	Linear nitrate, ν(N=O)	[42,68,70,72,81]
1300	Bridging bidentate nitrite, $\nu(NO_{2as})$	[70,72,73]
1230	Bridging bidentate nitrite, $\nu(NO_{2sym})$	
1160	Bridged N-coordinated nitrite, ν(N=O)	[70]
2146	—C≡N, ν(C≡N)	[75]
2280–2230	—NCO on Al^{3+}, out-of-phase ν(N=C=O)	[42,73,81]

Table 4
Assignments of peak position in DRIFT spectra results.

Phase	Assignment	Wavenumber (cm^{-1})
Ba [26,38,70,71,73,74]	Bridging and chelating bidentate nitrate	1650–1540
		1320–1210
		1050–1022
	Mododentate nitrate	1429–1424
		1332
	Linear nitrite	1420
	Monodentate nitrite	1440 and 1340
	Bridged bidentate nitrite	1300 and 1230
	–NCO on Ba, out-of-phase ν(N=C=O)	2160–2170
K [5,38,72]	Free nitrate ion	1750 and 1380
	Free nitrite ion	1260–1250
	Combination of nitrates denoted in this table	1560-1190
	Gas NO	1870
Carbon base adsorbates [5,34,71,72,75,76,81]	Bridged bidentate carbonate	1648, 1256 and 990
	Carboxylate ion	1599, 1310
	Chelating bidentate carbonate	1545, 1363
	Carbonate ion	1408, 1091
	Bridged CO	1975
	Pt bound CO	2000–2080
	Gas CO_2	2347

face [70]. In general, the assignment of the bands at region 1550–1200 cm^{-1} for the Pt–Ba catalyst is complicated due to the presence of different adsorbing species. These species exhibit a vibrational mode in the same region (Tables 3 and 4).

All spectra recorded during the accumulation phase (lines b in Fig. 10A) reveal the feature at 1760 cm^{-1}. The band at 1760 cm^{-1} can be assigned to the formation of nitrosyl M–ON^- or M–NO^- species [38,73]. This band can also be due to the free nitrate ion, especially considering the presence of this band at 1760 cm^{-1} together with band at 1380 cm^{-1}. The mode at ca. 2280 cm^{-1} observed during storage and regeneration steps (Fig. 10A) can arise from –NCO species weekly bonded with the catalyst surface [38,74,75]. The region 2390–2102 cm^{-1} was reported as characteristic for adsorbed nitrosonium ion (NO^+) [38]. This ionic species, however, decompose very quickly in the presence of H_2O formed in abundance during rich step under applied reaction condition. Therefore, this band was assigned to –NCO adsorbed onto alumina and/or Ba [42]. The weak features at high frequency region (above 2450 cm^{-1}) are most likely connected with C–H or N–H stretching of the surface compounds [75,76]. The intensity of –OH group region (ca. 3500–3800 cm^{-1}) during lean phase slightly increases with time (spectra b in Fig. 10), suggesting the formation of $Ba(OH)_2$ phase (band ca. 3650 cm^{-1}) [39]. At the end of lean phase, the increase in the band intensity at ca. 3730 cm^{-1} pointed out the formation of –OH groups over Al^{3+} [39]. During the reduction of stored nitrates/nitrites with H_2 (spectrum c in Fig. 10), the surface properties of the Pt–Ba catalyst were fully restored. The nitrites/nitrates were completely removed, and the intensity of bands in the –OH region slightly decreased. The negative peaks in the reduction spectrum in the nitrites/nitrates region (spectrum c vs. spectrum a in Fig. 10) suggest that during lean phase the removal of Ba carbonates took place, whose characteristic bands at 1100–1800 cm^{-1} overlap nitrites/nitrates region [34]. However, the amount of CO_2 produced during decomposition of Ba carbonates was not detected by MS.

In Fig. 10B, the spectra obtained for the Pt–Ba + soot mixture are presented. The band at ca. 1230 cm^{-1} arising from bidentate nitrites is observed only at the beginning of lean step. The predominant bands at 1310 and 1560 cm^{-1} are characteristic for bidentate nitrites. The small shoulder detected at 1480 cm^{-1} was assigned to linear nitrates over the support and the mode at 2320 cm^{-1} (last spectrum b in Fig. 10B) to the CO_2 adsorbed on surface species

[42]. The band at 2050 cm^{-1} is probably due to CO bonded on Pt sites, and the feature at 2130 cm^{-1} possibly arises from–CN groups, which are formed over Al or Ba sites [38,39,75]. For Pt–Ba + soot, the intensity of bands corresponding to –OH groups decreases, suggesting that $BaCO_3$ prevail over $Ba(OH)_2$. This is in good agreement with TEM, XRD and XPS characterization. Performed calculations show that at the beginning of simultaneous NO_x–soot removal, the NO_x accumulation decreases by 40% for Pt–Ba + soot. The amount of NO_x stored during first cycle at saturation point (lean phase, last spectrum b in Fig. 10B) was 7.312×10^{-4} mol/g_{cat}. However, during cyclic work condition, soot is consumed and the amount of nitrites/nitrates stored is the function of soot loading, as was also shown for TRM runs.

DRIFT spectra recorded during lean phase for the soot-free Pt–K catalyst (spectra b in Fig. 11A) in general show one dominant peak at 1250 cm^{-1} and weak bands at 1380, 1560 and 1760 cm^{-1}. The band at 1250 cm^{-1} can be assigned to the vibrational modes of free nitrite ion [38,72]. The peaks arising from free nitrate ions at 1380 and 1760 cm^{-1} and combination of bands at 1200–1600 cm^{-1} attributed to free nitrites, and Al-based nitrates are very weak. The data are in line with previous study [38,72], where a few features mostly connected to free nitrite and nitrate ions were detected. The study reports the presence of band at 1380 cm^{-1} as predominant feature, what correspond to free nitrate ion [72]. In our study, the predominant band, observed at 1250 cm^{-1}, arises from nitrite ions. This is due to lower oxidation capacity of the Pt–K system (as was mentioned above), and it is in good agreement with the TRM study.

For Pt–K, the perturbations in –OH region (3500-3800 cm^{-1}) are similar to that observed for the Pt–Ba soot-free catalyst. The band at ca. 3650 cm^{-1} can be assigned to –OH group bonded to K sites. The intensity of this band increases upon $NO_x + O_2$ admission (spectra b in Fig. 11A). The –OH groups connected to Al^{3+} sites (band at 3730 cm^{-1}) [39] are not detected during lean phase. However, while reduction was performed, the band at ca. 3650 and ca. 3730 cm^{-1}, characteristic for K–OH and Al–OH groups, respectively, appeared (spectrum c in Fig. 11A).

The decrease in the nitrites/nitrates bands intensity is observed for Pt–K + soot (Fig. 11B). The band at 1180 cm^{-1} arising from Al-based nitrite species [38,72] was evidenced only at the beginning of lean step (spectra b in Fig. 11B). The most intense bands at 1250 and 1560 cm^{-1} was assigned to free nitrite ions and Al-based nitrates [25,34,38,72]. The amount of nitrites/nitrates stored during first cycle at saturation point (lean phase, last spectrum b in Fig. 11B) was 5.672×10^{-4} mol/g_{cat}. For the Pt–K + soot mixture, the band at 3650 cm^{-1} can be assigned to −OH groups over the K surface species. The −OH groups connected to Al were not detected.

Fig. 11A and B shows the reduction step in H_2 atmosphere (spectra c in both figures) for the Pt–K catalyst with and without soot, respectively. The spectrum recorded for the soot-free catalyst reveals the presence of bands, which can be associated with –CN and –NCO groups formation (at 2160 and 2220 cm^{-1}, respectively), CO bonded on Pt sites (at 2060 cm^{-1}) and bridged CO (at 1980 cm^{-1}). There are also present wide features at 2390 and 1860 cm^{-1}, which can be assigned to adsorbed CO_2 and NO gas phase or gas phase-like, respectively [34,72]. The assignment of band at 1860 cm^{-1} is complex. Previous study indicated that the band at 1860 cm^{-1} can be associated with (i) vibration mode of mononitrosyls connected to Pt [44], (ii) the NO presence in gas phase [77] or (iii) NO weekly bonded to catalyst surface (gas phase-like) [38]. However, in our study the band intensity increased during rich phase under absence of NO (NO signal in MS profile was not detected). Therefore, under applied condition, the band at 1860 cm^{-1} may arise from CO bonded to Pt species [30,78–80]. The bands at 1860 and 2076 cm^{-1} are weaker during lean step, suggesting that upon H_2 reduction the Pt–K catalyst properties are not fully recovered [29,30]. It is worth noting that these bands were detected neither for the Pt–Ba nor for the Pt–Ba + soot catalyst (Fig. 10).

In general, DRIFT spectra recorded for soot-containing samples (Figs. 10B and 11B) show that soot modifies the NO_x storage capacity and diminishes the amount of the nitrites and nitrates retained on the Pt–Ba and Pt–K catalysts. Soot modifies also –OH region of both catalysts. However, these influences are a function of soot loading and are continuously changed during combined NO_x–soot removal process.

4. Conclusions

The Pt–Ba and Pt–K NSR catalysts have been evaluated in the simultaneous NO_x and soot removal under a cyclic work condition, and the soot effect on the NO_x storage and catalysts' regeneration with H_2 is reported. It was found that Pt–Ba and Pt–K are active in simultaneous NO_x and soot removal; however, K-containing samples present higher activity in terms of soot combustion. The onset for soot combustion in oxygen is in the range of 673–723 K and 573–623 K for the Pt–Ba and Pt–K catalysts, respectively. $NO + O_2$ mixture has a beneficial influence on the soot removal decreasing the soot ignition temperature by ca. 50 K, with respect to the combustion in oxygen. Performed study shows that the K or species connected to K are responsible for the increase in the catalytic activity in terms of soot oxidation. This increase in activity could be also connected with water retention and release, which improves the soot–catalyst contact leading the soot combustion at lower temperature.

It was found that for the Pt–Ba catalyst, the Pt^0/Pt_{ox} ratio value 0.7 is not affected during simultaneous NO_x–soot removal, therefore the cooperation between Pt and Ba in this system is considered to be better compared to Pt–K catalyst.

The nitrites/nitrates formation depends on the Pt–alkali component cooperation, although the overall NO_x storage capacity is apparently similar for both of the systems (saturation point). It has been established via DRIFTS–TRM study that the NO_x storage proceeds through nitrites/nitrates route. Under a prolonged exposure to oxidation condition, nitrites are transformed into nitrates species, probably involving NO_2 molecules. During the reduction of stored nitrites/nitrates with H_2, the catalyst properties are fully restored (nitrite/nitrate species are completely removed) for the Pt–Ba catalyst, whereas the regeneration process is limited for Pt–K. It was found that this could be related to the –NCO, –CN group formation over catalyst-active species and/or CO embedded in Pt sites. In general, the storage properties of the Pt–Ba and Pt–K catalysts are hindered by the soot presence.

Acknowledgments

I.A.S.P. acknowledges Spanish Ministry of Education MEC for the FPI Grant, project CTQ 2006-09780/PPQ. Special thanks to Prof Luca Lietti Politecnico di Milano for TRM.

References

[1] I. Atribak, I. Such-Basanez, A. Bueno-Lopez, A. Garcia-Garcia, J. Catal. 250 (2007) 75.
[2] A. Bueno-Lopez, M.J. Illan-Gomez, C.S.-M.d. Lecea, Appl. Catal. A 302 (2006) 244.
[3] P. Gilot, M. Guyon, R. Stanmore, Fuel 76 (1997) 507.
[4] E.F. Iliopoulou, A.P. Evdou, A.A. Lemonidou, I.A. Vasalos, Appl. Catal. A 274 (2004) 179.
[5] T. Lesage, J. Saussey, S. Malo, M. Hervieu, C. Hedouin, G. Blanchard, M. Daturi, Appl. Catal. B 72 (2007) 166.
[6] R. Matarrese, L. Castoldi, L. Lietti, P. Forzatti, Top. Catal. 42–43 (2007) 293.
[7] R. Matarrese, L. Castoldi, L. Lietti, P. Forzatti, Catal. Today 136 (2008) 11.

[8] S.S. Mulla, S.S. Chaugule, A. Yezerets, N.W. Currier, W.N. Delgass, F.H. Ribeiro, Catal. Today 136 (2008) 136.
[9] U. Wagner, P. Eckert, U. Spicher, The 12th International Symposium on Transport Phenomena and Dynamics of Rotating Machinery, Honolulu, Hawaii, 2008.
[10] P. Ciambelli, P. Corbo, P. Parrella, M. Scialo, S. Vaccaro, Thermochim. Acta 162 (1990) 83.
[11] J.-Y. Luo, M. Meeng, Y.-Q. Zha, Y.-N. Xie, T.-D. Hu, J. Zhang, T. Liu, Appl. Catal. 78 (2008) 38.
[12] C.L.M. Scholz, B.H.W. Maes, M.H.J.M.d. Croon, J.C. Schouten, Appl. Catal. A 332 (2007) 1.
[13] Y. Teraoka, K. Nakano, W. Shangguan, S. Kagawa, Catal. Today 27 (1996) 107.
[14] S.J. Jelles, R.R. Krul, M. Makkee, J.A. Moulijn, Catal. Today 53 (1999) 623.
[15] J. Li, J. Hao, L. Fu, T. Zhu, Z. Liu, X. Cui, Appl. Catal. A 265 (2004) 43.
[16] I. Nova, L. Lietti, P. Forzatti, Catal. Today 136 (2008) 128.
[17] A.E. Palomares, A. Uzcategui, A. Corma, Catal. Today 137 (2008) 261.
[18] G.A. Stratakis, A.M. Stamateleos, Combust. Flame 132 (2003) 157.
[19] K. Tashiro, S. Ito, A. Oba, T. Yokomizo, JSAE Rev. 16 (1995) 131.
[20] C. Verrier, J.H. Kwak, D.H. Kim, C.H.F. Peeden, J. Szanyi, Catal. Today 136 (2008) 121.
[21] B.A.A.L. Setten, M. Makee, J.A. Moulijn, Catal. Rev. 43 (2001) 489.
[22] J.J. Yu, Y.X. Tao, C.C. Liu, Z.P. Hao, Z.P. Xu, Environ. Sci. Technol. 41 (2007) 1399.
[23] W.S. Epling, L.E. Campbell, A. Yezerets, N.W. Currier, J.E. Parks, Catal. Rev. 46 (2004) 163.
[24] K. Nakatani, S. Hirota, S. Takeshima, K. Itoh, T. Tanaka, K. Dohmae, SAE Article, 01-0957, 2002.
[25] J.A. Anderson, B. Bachiller-Baeza, M. Fernandez-Garcia, Phys. Chem. Chem. Phys. 20 (2003) 4418.
[26] E. Fridell, M. Skoglundh, B. Westerberg, S. Johansson, G. Smedler, J. Catal. 183 (1999) 196.
[27] S. Morandi, F. Prinetto, G. Ghiotti, M. Livi, A. Vaccari, Microporous Mesoporous Mater. 107 (2008) 31.
[28] L. Zhiming, I.W. Seong, Catal. Rev. 48 (2006) 43.
[29] I.S. Pieta, I. Malpartida, M. Garcia-Dieguez, M.C. Herrera, M.A. Larrubia, L.J. Alemany, Conference Proceedings XL Annual Polish Conference on Catalysis 'Catalysis for Society' Krakow, Poland, 2008, ISBN: 978-83-60514-06-1, 2008.
[30] I.S. Pieta, I. Malpartida, M. Garcia-Dieguez, M.C. Herrera, M.A. Larrubia, L.J. Alemany, Conference Proceedings Simposio Iberoamericano de Catalisis SICAT, Malaga, Spain. 2008, ISBN: 978-984-691-4239-4239, 4117.
[31] L. Castoldi, R. Matarrese, L. Lietti, P. Forzatti, Appl. Catal. B 64 (2006) 25.
[32] P. Forzatti, and L. Lietti, Cat. Today, in press, doi:10.1016/j.cattod.2008.11.023.
[33] L. Lietti, I. Nova, P. Forzatti, J. Catal. 257 (2008) 270.
[34] W.S. Epling, C.H.F. Peden, J. Szanyi, J. Phys. Chem. 112 (2008) 10952.
[35] V.G. Milt, M.A. Peralta, M.A. Ulla, E.E. Miró, Catal. Commun. 8 (2007) 765.
[36] N. Nejar, M. Makkee, M.J. Illan-Gomez, Appl. Catal. B 75 (2007) 11.
[37] A. Setabudi, M. Makkee, J.A. Moulijn, Appl. Catal. B 50 (2004) 185.
[38] K.I. Hadjiivanov, Catal. Rev. – Sci. Eng. 42 (2000) 71.
[39] I. Malpartida, M.A. Larrubia, L.J. Alemany, E. Finocchio, G. Busca, Appl. Catal. B 80 (2008) 214.
[40] M.J. Conrado, J.A. Anderson, J. Mol. Catal. A 138 (1999) 83.
[41] H.Y. Huang, R.Q. Long, R.T. Yang, Energy Fuels 15 (2001) 205.
[42] Z. Liu, J.A. Anderson, J. Catal. 224 (2004) 18.
[43] H. Mahzoul, J.F. Brilhac, P. Gilot, Appl. Catal. B 20 (1999) 47.
[44] F. Prinetto, G. Ghiotti, I. Nova, L. Lietti, E. Tronconi, P. Forzatti, J. Phys. Chem. B 105 (2001) 12732.
[45] L. Castoldi, R. Matarrese, L. Lietti, P. Forzatti, Appl. Catal. B 90 (2009) 278.
[46] R. Bɔchel, R. Strobel, F. Krumeich, A. Baiker, S.E. Pratsinis, J. Catal. 261 (2009) 201.
[47] K. Krishna, M. Makkee, Catal. Today 114 (2006) 48.
[48] Q. Li, M. Meng, Z.Q. Zou, X.G. Li, Y.Q. Zha, J. Hazard. Mater. 161 (2009) 366–372.
[49] J. Jung, J.H. Lee, S. Song, K.M. Chun, IJAT 9 (2008) 423.
[50] R. Zhang, W. Yang, J. Xue, B. Chen, Catal. Lett. 132 (2009) 10.
[51] C. Alcala-Jornod, H.v.d. Bergh, M.J. Rossi, PCCP 2 (2000) 5584.
[52] N.M. Persjanseva, O.B. Popovicheva, A.M. Starik, M.E. Trukhin, N.K. Shonija, Tech. Phys. Lett. 26 (2000) 50.
[53] S. Picaud, B. Collignon, P.N.M. Hoang, J.C. Rayez, PCCP 10 (2008) 6998.
[54] O.B. Popovicheva, N.M. Persjanseva, N.K. Shonija, P. DeMott, K. Koehler, M. Petters, S. Kreidenweis, V. Tishkova, B. Demirdjian, J. Suzanne, PCCP 10 (2008) 2332.
[55] S. Seisel, Y. Lian, T. Keil, M.E. Trukhin, R. Zellner, PCCP 6 (2004) 1926.
[56] C. Janiak, R. Hoffmann, P. Sjovall, B. Kasemo, Langmuir 9 (1993) 3427.
[57] S.G. Chen, R.T. Yang, Energy Fuels 11 (1997) 421.
[58] D.W. MacKee, C.I. Spiro, P.G. Kosky, E.J. Lamb, Fuel 64 (1985) 805.
[59] J.A. Moulijn, F. Kapteijn, Carbon 33 (1995) 1155.
[60] J.P.A. Neeft, M. Makkee, J.A. Moulijn, Chem. Eng. J. 64 (1996) 295.
[61] J.P.A. Neeft, M. Makkee, J.A. Moulijn, Appl. Catal. B 8 (1996) 57.
[62] M.L. Pisarello, V.G. Milt, M.A. Peralta, C.A. Querini, E.E. Miro, Catal. Today 75 (2002) 465.
[63] A. Setiabudi, M. Makkee, J.A. Moulijn, Appl. Catal. B 50 (2004) 185.
[64] N. Russo, S. Furfori, D. Fino, G. Saracco, V. Specchia, Appl. Catal. B 83 (2008) 85.
[65] B.R. Stanmore, J.F. Brilhac, P. Gilot, Carbon 39 (2001) 2247.
[66] M.A. Peralta, V.G. Milt, L.M. Cornaglia, C.A. Querini, J. Catal. 242 (2006) 118.
[67] R. Jimnez, X. Garcia, C. Collier, P. Ruitz, A.L. Gordon, Appl. Catal. A 314 (2006) 81.
[68] B.R. Kromer, L. Cao, L. Cumaranatunge, S.S. Mulla, J.L. Ratts, A. Yezerets, N.W. Currier, F.H. Ribeiro, W.N. Delgass, J.M. Caruthers, Catal. Today 136 (2008) 93–103.
[69] S. Balcon, C. Potvin, L. Salin, J.F. Tempere, G. Djega-Mariadassou, Catal. Lett. 60 (1999) 39.
[70] C. Sedlmar, K. Seshan, A. Jentys, J.A. Lercher, J. Catal. 214 (2003) 308.
[71] Y. Ji, T. Toops, J.A. Pihl, M. Crocker, Appl. Catal. B 91 (2009) 329.
[72] T. Toops, D.B. Smith, W.P. Partridge, Appl. Catal. B 58 (2005) 245.
[73] A.L. Kustov, M. Makkee, Appl. Catal. B 88 (2009) 263.
[74] P. Broqvist, H. Gronbeck, E. Fridell, J. Phys. Chem. B 108 (2004) 3523.
[75] B.I. Mosqueda-Jimenez, A. Jentys, K. Sehshan, J.A. Lercher, Appl. Catal. B 46 (2003) 189.
[76] E. Finocchio, G. Busca, Catal. Today 70 (2001) 213.
[77] I. Malpartida, M.O. Guerrero-Perez, M.C. Herrera, M.A. Larrubia, L.J. Alemany, Catal. Today 126 (2007) 162.
[78] G. Busca, V. Lorenzelli, Mater. Chem. 7 (1982) 89.
[79] NITS, National Technical Information Service DE92013242, 1992.
[80] J.B. Peri, J. Phys. Chem. 70 (1966) 3168.
[81] N. Macleod, R.M. Lambert, Appl. Catal. B 46 (2003) 483.